Magnetic field variations in the Jovian magnetotail induced by solar wind dynamic pressure enhancements

Chihiro Tao,[1] Ryuho Kataoka,[2] Hiroshi Fukunishi,[1] Yukihiro Takahashi,[1] and Takaaki Yokoyama[3]

Received 6 December 2004; revised 11 July 2005; accepted 19 July 2005; published 11 November 2005.

[1] In order to understand the response of the Jovian magnetosphere to solar wind dynamic pressure enhancements, we investigate magnetic field variations observed by the Galileo spacecraft. The lack of solar wind monitoring just upstream of the Jovian magnetosphere is overcome by simulating a one-dimensional magnetohydrodynamic (MHD) propagation of the solar wind from the Earth. We identify the events with an increase of the solar wind dynamic pressure >0.25 nPa at the Jovian orbit. Characteristic magnetic field variations are found in the Jovian magnetosphere for all of the nine events. The rectangular waveform due to the Jovian rotation disappears for eight of the nine events. Magnetic field disturbances in the frequency range from 0.3 to 10 mHz are enhanced simultaneously. The maximum amplitude of the disturbances is in proportional to the maximum amplitude of the solar wind dynamic pressure. We suggest that the current sheet is greatly deformed and reconnection bursts are induced under the compressed magnetosphere.

Citation: Tao, C., R. Kataoka, H. Fukunishi, Y. Takahashi, and T. Yokoyama (2005), Magnetic field variations in the Jovian magnetotail induced by solar wind dynamic pressure enhancements, *J. Geophys. Res.*, *110*, A11208, doi:10.1029/2004JA010959.

1. Introduction

[2] Magnetic field measurements have been the most important and fundamental technique required for the investigation of the electromagnetic environment of planetary magnetospheres since the beginning of space research. In the Jovian magnetosphere, the magnetic field has been observed by the Pioneer 10 and 11, Voyager 1 and 2, Ulysses, Galileo, and Cassini missions. The most prominent perturbation is a rectangular magnetic field waveform with a 10-hour period. This waveform is the result of a current sheet crossing caused by the tilt of the Jovian dipole moment to the spin axis. *Khurana* [1992, 2001] derived a current sheet model from the magnetic field data obtained by Voyager 2. This modeled current sheet lies in the magnetic dipole equator at 15–30 R_J, where R_J is the radius of Jupiter, and becomes parallel to the Jupiter's rotational equator at >60 R_J. Magnetic field disturbances in the mHz band are observed simultaneously with the rectangular waveforms. From Voyager 2 data, obtained at 18–32 R_J, the magnetic field disturbances were interpreted as a Kolmogorov-type turbulence because the power spectral density decreases with frequency by a power law index of −5/3 [*Glassmeier*, 1995].

[3] One of the most fundamental approaches in diagnosing the electromagnetic properties of magnetosphere is to investigate its response to an enhancement of the solar wind dynamic pressure. *Smith et al.* [1978] showed that the Pioneer 10 and 11 spacecraft made several crossings of the magnetopause at varying distances of 50–100 R_J, corresponding to solar wind dynamic pressure enhancements. Recently, when the Cassini spacecraft was available as an upstream solar wind monitor, *Gurnett et al.* [2002] showed an event in which interplanetary shocks could trigger increases in both hectometric radio emission and extreme ultraviolet auroral emission. For the same event, *Hanlon et al.* [2004] showed that increases and decreases of the solar wind dynamic pressure changed the configuration of magnetic field in the Jovian magnetosphere. Their results are consistent with the concept of conservation of angular momentum, which supports the theory of *Southwood and Kivelson* [2001] and *Cowley et al.* [2003a].

[4] The purpose of this study is to elucidate the fundamental response of the Jovian magnetotail to solar wind dynamic pressure enhancements. The lack of solar wind monitoring just upstream of the Jovian magnetosphere makes such analysis problematic. In order to overcome this problem, we have simulated a one-dimensional magnetohydrodynamic (MHD) propagation of the solar wind measured at the Earth. The solar wind model used for this study and its verification are described in section 2. We use Galileo spacecraft data to monitor the response of the

[1]Department of Geophysics, Tohoku University, Miyagi, Japan.
[2]National Institute of Information and Communications Technology, Tokyo, Japan.
[3]Department of Earth and Planetary Science, University of Tokyo, Tokyo, Japan.

0148-0227/05/2004JA010959$09.00

magnetic fields within the Jovian magnetosphere. Analysis of magnetic field data, obtained results, and discussion are presented in sections 3, 4, and 5, respectively. In section 6, we conclude that there are several types of responses associated with Jovian magnetic field.

2. Solar Wind Simulation

2.1. Solar Wind Model

[5] The solar wind is modeled as an ideal MHD fluid affected by solar gravity in a one-dimensional spherically symmetric coordinate system. The one-dimensional ideal MHD equations are solved using the Coordinated Astronomical Numerical Software (CANS), which is based on an explicit finite difference upwind scheme. The stabilizing of the numerical integration of hyperbolic MHD equations and improvement of accuracy are achieved by applying the Total Variation Diminishing (TVD) numerical flux based on the Monotonic Upstream Scheme for Conservation Laws (MUSCL) approach with a linearized Riemann solver. The source code is available at the website http://www.astro.phys.s.chiba-u.ac.jp/netlab/pub/index.html.

[6] We take the Cartesian coordinate system in which the x axis points outward from the Sun in the equatorial plane, the z axis points northward, and the y axis completes the orthogonal triad. We assume that the z component of the magnetic field is zero constant as a simplification. MHD equations in a conservative form are given in the CGS Gauss system as

$$\frac{\partial}{\partial t}(\rho S) + \frac{\partial}{\partial x}(\rho v_x S) = 0 \tag{1}$$

$$\frac{\partial}{\partial t}(\rho v_x S) + \frac{\partial}{\partial x}\left[\left(\rho v_x^2 + p + \frac{B^2}{8\pi} - \frac{B_x^2}{4\pi}\right)S\right] = \rho\left[g_x + \left(v_y^2 - \frac{B_y^2}{4\pi\rho}\right)\frac{1}{R}\frac{dR}{dx}\right]S + \left(p + \frac{B^2}{8\pi}\right)\frac{dS}{dx} \tag{2}$$

$$\frac{\partial}{\partial t}(\rho v_y R S) + \frac{\partial}{\partial x}\left[\left(\rho v_x v_y - \frac{B_x B_y}{4\pi}\right)RS\right] = 0 \tag{3}$$

$$\frac{\partial}{\partial x}(B_x S) = 0 \tag{4}$$

$$\frac{\partial}{\partial t}\left(\frac{B_y S}{R}\right) - \frac{\partial}{\partial x}\left(\frac{(-v_x B_y + v_y B_x)S}{R}\right) = 0 \tag{5}$$

$$\frac{\partial}{\partial t}\left[\left(\frac{1}{2}\rho v^2 + \frac{p}{\gamma - 1} + \frac{B^2}{8\pi}\right)S\right] + \frac{\partial}{\partial x}\left[\left\{v_x\left(\frac{1}{2}\rho v^2 + \frac{\gamma p}{\gamma - 1}\right) - \frac{1}{4\pi}(B_y(-v_x B_y + v_y B_x))\right\}S\right] = \rho g_x v_x S, \tag{6}$$

where ρ, v, B, and p are the mass density, velocity, magnetic field, and thermal pressure, respectively. Specific heat ratio γ is taken to be 7/5 in this simulation. Solar gravitational force is $g_x = -GM/x^2$, where G is the gravitational constant and M is the solar mass. The unit surface S is defined as x squared. $R(x) \approx x$ is a distance from the solar rotation axis.

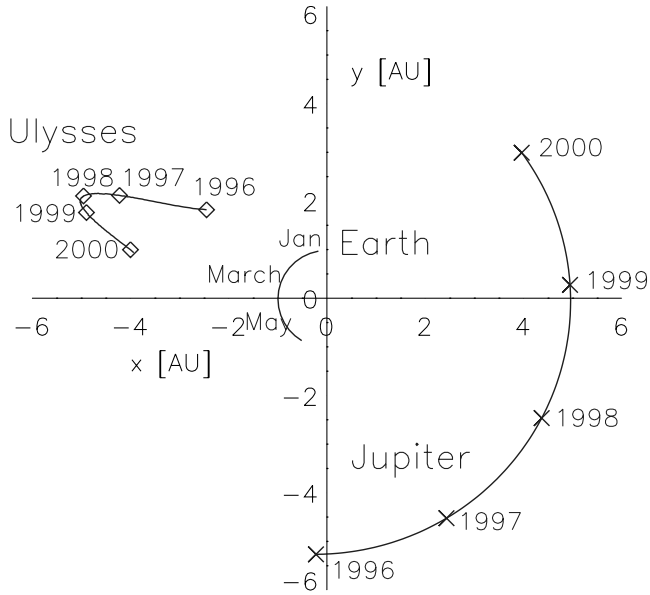

Figure 1. The location of Ulysses (a solid line with diamonds) and Jupiter (a solid line with crosses) seen from north for the period from 1996 to 2000 containing our verification terms, 1998 and 1999. Earth orbit from 1 January to 1 June is represented by a line without marks. The horizontal x axis extends toward the first point of Aries. The z axis, pointing upward through the paper, is aligned with the solar rotation axis. The vertical y axis completes a right-handed set. The distance is given by astronomical units (AU).

[7] The time step and grid spacing are chosen to be 10 s and 1/300 AU, respectively. The outer boundary is at 8 AU where the derivatives of all physical quantities go to zero. The inner boundary is placed at 1 AU where the solar wind data measured at the Earth is used as the input. One-hour average data obtained from the OMNI website (http://nssdc.gsfc.nasa.gov/omniweb/) is linearly interpolated for every time step to meet the CFL condition. In order to satisfy equation (4), the inner B_x value drops as $1/x^2$ as the plasma parcel propagates antisunward. In this simulation, in order to minimize the effect of B_x, we fix the B_x amplitude as approximately 1/1000 of the other component. Since the averaged B_x value during the simulated interval is positive, we select B_x = 0.001 nT at the inner boundary. It is confirmed in advance that dynamic pressure variations are not sensitive to B_x values by applying B_x = −10, −1, 0, 0.001, 1, and 10 nT as the inner values against three pressure pulses from 5 March to 5 April 1998. As the result, the arrival time and the maximum amplitude change 15 hours and 28% at most, respectively, depending on the fixed B_x values. From our MHD model, the output parameters are obtained at 5.2 AU. In order to adopt our one-dimensional (1-D) simulation data, we have to make a correction about the Earth-Sun-Jupiter (or Earth-Sun-Ulysses) geometry. This correction is estimated as $\Delta t = -\phi/\Omega$, where ϕ is the Earth-Sun-Jupiter angle and Ω is an angular velocity of the Sun. Another correction is necessary for the fact that the actual radial distances of Jupiter (or Ulysses) from the Sun are slightly different from 5.2 AU. We correct this effect

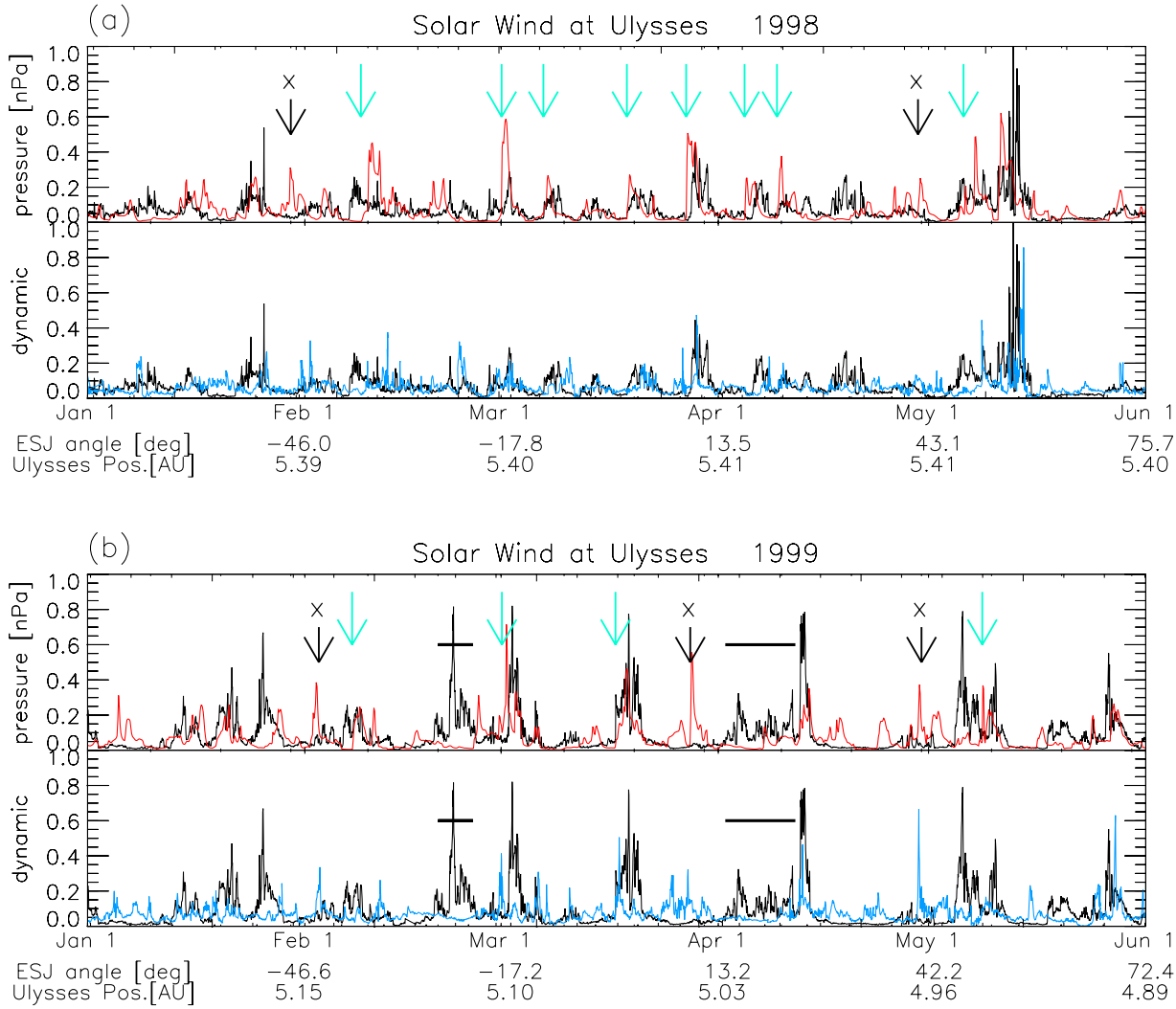

Figure 2. Solar wind dynamic pressure variations for the time intervals (a) 1 January 1998 to 1 June 1998 and (b) 1 January 1999 to 1 June 1999. Data from Ulysses observation, solar wind MHD simulation, and advection shift method are shown by black, red, and blue lines, respectively. Vertical green arrows indicate the arrival time of large-amplitude pressure pulses >0.25 nPa as predicted by MHD simulation. Pulses indicated by black arrows with crosses show the events without correspondence between observation and simulation. Black bars show the intervals affected by gaps of input data at 1 AU.

by shifting solar wind structure assuming that they propagate with the constant solar wind speed.

2.2. Verification

[8] We have compared the solar wind profile at Jupiter's orbit obtained from our MHD simulation with the actual data measured by the Ulysses spacecraft. In order to verify our simulation, we need to see the data obtained around the Jovian orbit at 5.2 AU. There are two Ulysses orbits where the radial distance from the Sun is within 5.2 ± 0.3 AU as shown in Figure 1. Jupiter was located on the opposite side of the Sun with respect to Ulysses' location during these approaches. Figure 2 shows the dynamic pressure variations obtained from the Ulysses observations (black trace) and from our simulation (red trace). It is found that pressure pulses with large amplitudes of >0.25 nPa are reasonably well predicted as indicated by green arrows when ϕ is <50°, where ϕ is the Earth-Sun-Ulysses angle in this verification instead of the Earth-Sun-Jupiter angle. Dynamic pressure pulses in five events indicated by black arrows with crosses do not have corresponding pulses in the observations. It should also be noted that two intervals indicated by black bars are unreliable due to the data gaps of solar wind observation at 1 AU. Just for comparison, the result of arrival time prediction based on a simple advection shift method of *Vennerstrom et al.* [2003] is also plotted in Figure 2 (blue trace). In this method, assuming the constant solar wind velocity during radial propagation from the Earth to the planet, the delay time is estimated as $\Delta t = (r_{Jupiter} - r_{Earth}/v_{sw})$, where r is the heliospheric distance from the center of the Sun to the respective planets and v_{sw} is the solar wind speed measured at 1 AU. Additionally, the Earth-Sun-Ulysses geometry is approximated in the same way as is done in the MHD mothod. It is assumed that the density varies as $1/r^2$ and that the solar wind speed is constant with r during the radial propagation.

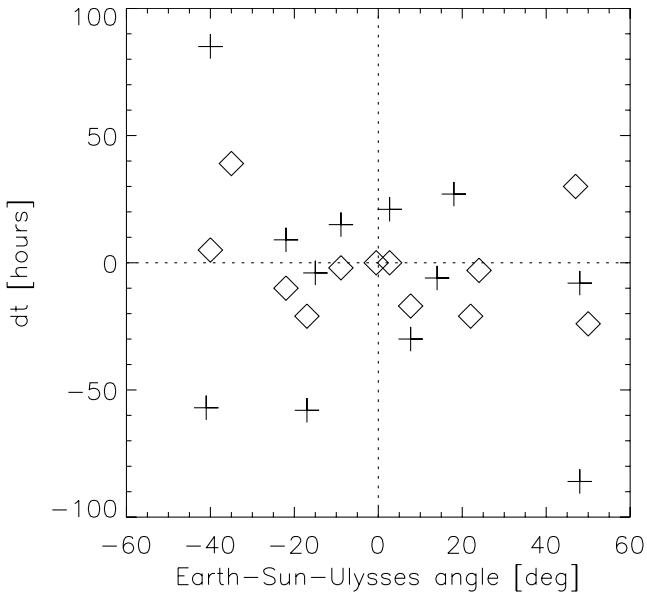

Figure 3. A scatter plot of the prediction errors in pressure enhanced time (vertical) versus the Earth-Sun-Ulysses angle (horizontal) for 12 dynamic pressure enhancement events. Events shown by diamonds and crosses are estimated from the MHD simulation and the advection shift method, respectively.

[9] The model is verified more accurately by focusing on the arrival times and absolute values for the associated 12 pressure enhancements. As shown in Figure 3, the prediction error of the MHD simulation is found to be better compared with that of the advection shift method. The standard deviations of the MHD simulation and the advection shift are 19.7 and 45.7 hours, respectively. It is concluded from Figure 3 that the prediction error of the MHD simulation is at most 2 days when ϕ is <50°.

[10] In Figure 4, the maximum values of the modeled dynamic pressure of the solar wind events observed in Figure 2 are plotted against the maximum values of the associated events measured by Ulysses. A good positive correlation exists between the result from each model and the observed data. Linear correlation coefficients of the MHD and advection models are 0.66 and 0.86, respectively.

[11] We should consider that there are some limitations in the use of solar wind parameters predicted by the MHD simulation. The first one is that five of the 17 predicted pressure enhancement events have not arrived at the orbit of Jupiter. This result means that there is ~29% ambiguity in the event selection itself. It would reduce the number of comparable pressure enhancement events. Second, when the prediction error in the arrival time and the duration of pressure pulses are comparable, we cannot identify the increasing or decreasing phase of solar wind dynamic pressure. Third, since the B_x and B_z components of the interplanetary magnetic field (IMF) are fixed in this simulation, we cannot discuss the effect of IMF variation on the Jovian magnetosphere.

3. Magnetic Field Data Analysis

[12] Continuous magnetic field measurements in the vicinity of the Jovian equatorial plane were made by the Galileo spacecraft between 1995 and 2003. The Galileo data is available at the web site of Planetary Data System (http://www.igpp.ucla.edu/ssc/pdsppi/index.htm). Magnetometer (MAG) real time survey (RTS) data [*Kivelson et al.*, 1992] is used in this analysis and a time resolution of 24 s makes it possible to investigate magnetic disturbances in the ultra-low frequency (ULF) range of <20 mHz. Three criteria are adopted to select the events listed in Table 1: the Earth-Sun-Jupiter angle ϕ is <50°, to keep the reliability of predicted solar wind parameters, the maximum solar wind dynamic pressure on the magnetosphere is >0.25 nPa, and MAG RTS data obtained inside the magnetosphere is available over a period >5 days including each pressure enhancement event.

[13] The purpose of this analysis is to obtain the temporal variations and wave structures assuming the spacecraft velocity is negligible. The actual movement of the spacecraft makes it impossible to distinguish between temporal and spatial variations from observed data. Galileo surveyed the magnetotail around apoapsis before March 2000, which is expected to reduce the above confusion. For this reason, we have analyzed the data obtained before March 2000 in this study. Figure 5 shows the locations of Galileo during the analyzed events.

[14] The Fast Fourier Transform (FFT) method is applied to obtain dynamic power spectra in the ULF range. First, a running average over a 128 × 24 s window interval is subtracted to remove a trend curve. The window interval for each FFT is also fixed as 128 × 24 s. The data window is successively advanced by 32 × 24 s. Thus dynamic power spectra in the frequency range ~0.3 to ~20 mHz are obtained.

[15] The strength of the magnetic field disturbance in the ULF range is defined hereafter as an absolute value of the

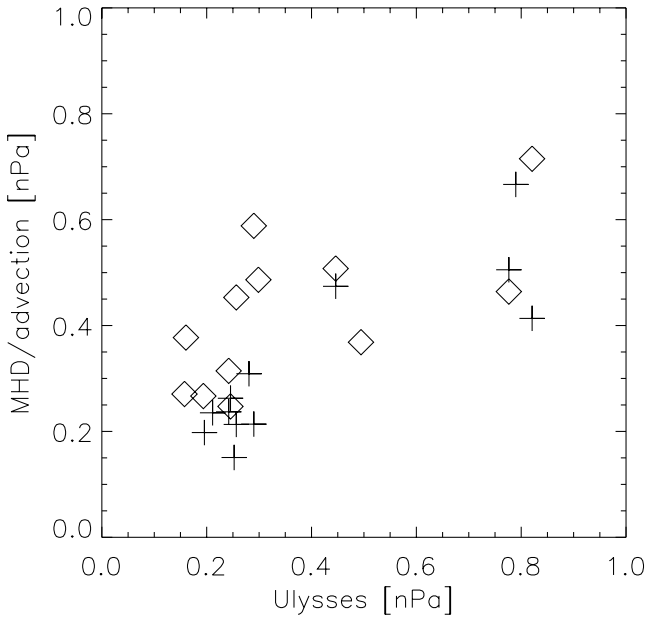

Figure 4. A scatter plot of predicted maximum values (vertical) versus actual values (horizontal) for 12 dynamic pressure enhancement events. Similar to Figure 3, the values from the MHD model and the advection method are represented by diamonds and crosses, respectively.

Table 1. Event List of Simulated Pressure Enhancements >0.25 nPa[a]

Event	Orbit	Date	ϕ	Galileo Location
1	1	1996/8/13	20	(−59, −102, −8.8)
2	9	1997/7/15	−41	(−113, 19, −0.4)
3	9	1997/8/5	−19	(−143, −11, −0.5)
4	9	1997/8/17	−7	(−134, −27, −0.5)
5	9	1997/8/26	−2	(−113, −37, −0.5)
6	10	1997/9/23	26	(−53, 21, 0.2)
7	10	1997/10/12	42	(−98, −14, 0.2)
8	10	1997/10/21	50	(−82, −32, 0.05)
9	16	1998/8/18	−42	(−123, 9.7, 1.0)

[a]Listed data from left to right are event number, orbit number, predicted arrival date at the Jupiter orbit, Earth-Sun-Jupiter angle, and the Jupiter Solar Ecliptic (JSE) position of the Galileo spacecraft in units of Jupiter radii where 1 R_J = 71,492 km.

magnetic field disturbance after removal using a running average window with a 128 × 24 s interval. The closer Galileo approaches to Jupiter, the stronger become the magnetic field disturbances. In order to compare the strengths of magnetic field disturbances at different distances from Jupiter, we normalize the strengths by averaged absolute values of the magnetic field radial component.

4. Results

[16] The relationships between solar wind dynamic pressure enhancements predicted from the MHD simulation and the time series of the magnetic field data observed by Galileo are summarized for nine events in Figure 6. Plotted panels from top to bottom for each event in Figure 6 are the solar wind dynamic pressure, the B_r, B_θ, and B_ϕ components of magnetic field waveforms in the Jupiter Solar Equatorial (JSE) spherical coordinate system, and the strength and dynamic spectrum of the B_θ component in the ULF range of 0.3−20 mHz. Here, the B_r, B_θ, and B_ϕ components represent the magnetic field in the radial, colatitude, and azimuthal directions, respectively.

[17] As a typical example, event 8 in orbit 10 for the 10-day period starting 16 to 26 October is shown in Figure 6h. It is found that the traces of the B_r and B_ϕ components deviate from a steady rectangular waveform for the 2-day interval starting 21 to 23 October when a predicted dynamic pressure enhancement arrives. Furthermore, as shown in the lower two panels, the ULF amplitude of the B_θ component is enhanced without clear spectral peaks. This enhancement is also detected in the B_r and B_ϕ components.

[18] Similar signatures can be identified for other solar wind pressure enhancement events. Deviations from the rectangular waveform are indicated by red bars in each plot except for event 6 in Figure 6f. This event 6 is observed at 57 R_J during the closest approach of Galileo to Jupiter as shown in Figure 5. Enhancements of ULF disturbances are found in events 2−9 judged by the B_θ strength becoming >2σ corresponding with solar wind pressure enhancements, where σ is a standard deviation of the B_θ strength during 10 days.

[19] It is interesting that the rectangular waveform of event 1 shown in Figure 6a is different from the waveform of other events, i.e., signatures of the current sheet crossings are not clear. This is due to the position of Galileo close to the dawnside magnetopause as shown in Figure 5. In this particular event, a trapped continuum radiation disappeared in the data observed by the Plasma Wave Subsystem (PWS) instrument aboard Galileo. The trapped continuum radiation is observed in the frequency range from about 0.5 to 10 kHz and is present (absent) when the spacecraft is inside (outside) the magnetosphere [see *Gurnett et al.*, 2002, and references therein]. The period in which this radiation disappeared is denoted by green bars in Figure 6a. It suggests that Galileo is possibly outside the magnetosphere for two intervals (on 15 and 16 August) due to magnetospheric compression caused by solar wind dynamic pressure enhancement.

5. Discussion

[20] In section 4, we have shown that (1) the rectangular waveform with the 10-hour Jovian rotation period disappeared for eight of the nine events, and (2) enhancements of magnetic field disturbances in the ULF range occurred for eight of the nine events, in response to the solar wind dynamic pressure enhancements. The generation mechanism of these two types of responses is discussed below.

[21] If the compression of the magnetosphere is the main energy source of the enhancement of ULF disturbances, there should be a correlation between the amplitude of ULF disturbances and solar wind dynamic pressure. In Figure 7, we show scatter plots of the maximum solar wind dynamic pressure and the maximum

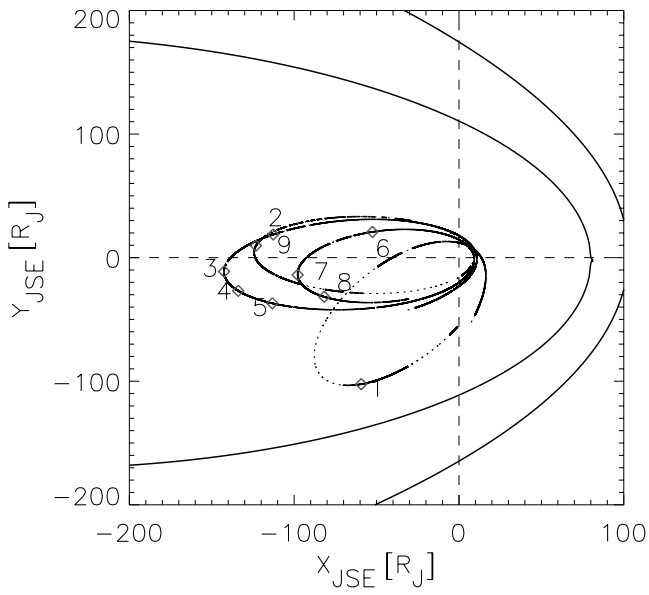

Figure 5. Galileo's locations during the nine events of solar wind pressure enhancements. Jupiter is located at the origin and sunward direction is right-hand. The shape of the magnetopause and that of bow shock have been estimated from the empirical model [*Joy et al.*, 2002]. The terms with RTS data are indicated by solid lines of the Galileo's trajectory. Each number corresponds to the event number in Table 1.

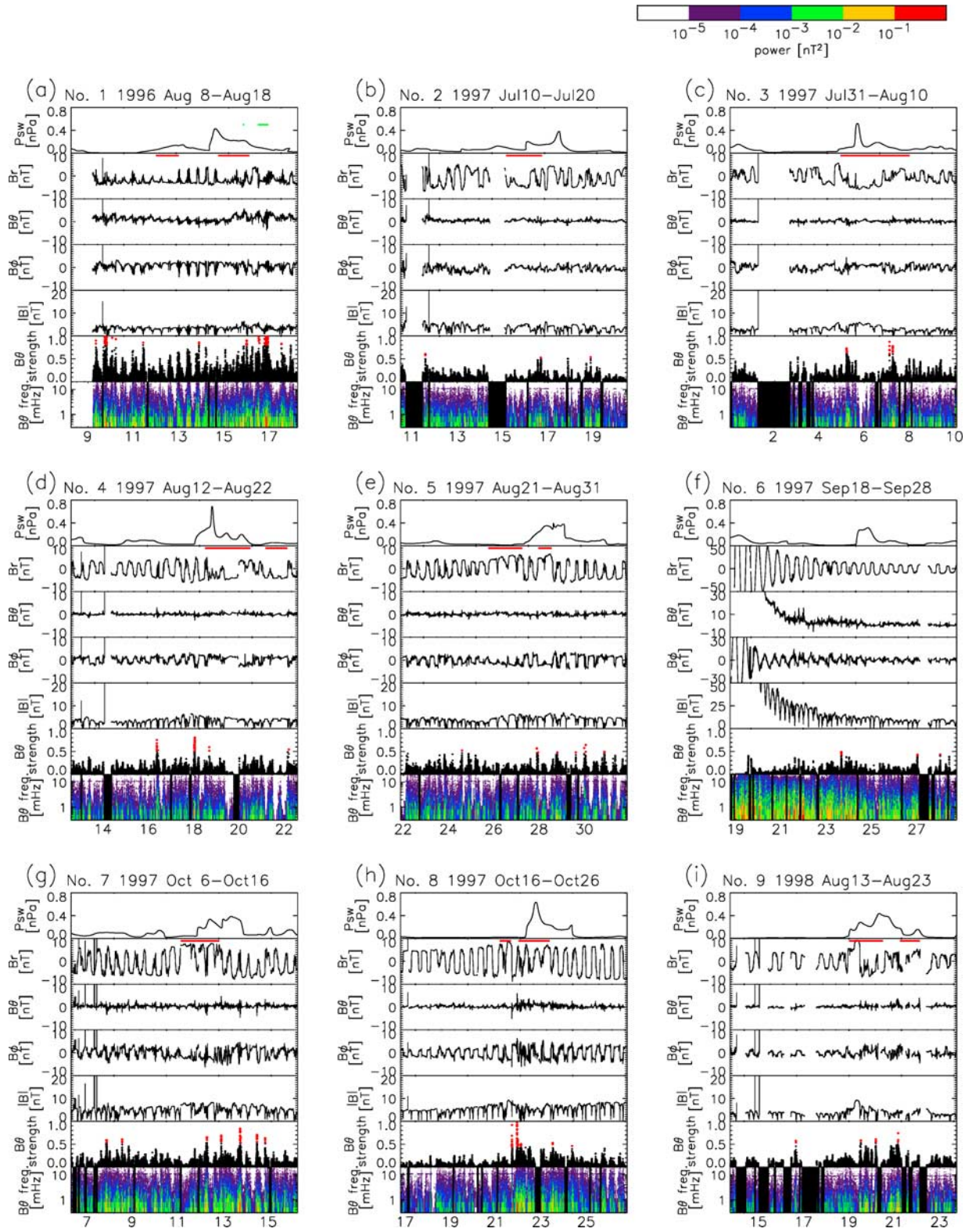

Figure 6. Summary of dynamic pressure enhancement events predicted from solar wind simulation, Jovian magnetic field traces in the JSE spherical coordinate system, and the strength and dynamic spectra of the magnetic field colatitude component in the ULF range. (a), (b), . . ., (i) Corresponds to events 1, 2, . . ., 9. Red bars indicate the term when the waveform of B_r is deviated from the regular rectangular waveform. Green bars in Figure 6a represent the term when the trapped continuum radiation disappears. Red dots in the sixth panel indicate that the values become >2σ, where σ is a standard deviation of the B_θ strength during 10 days.

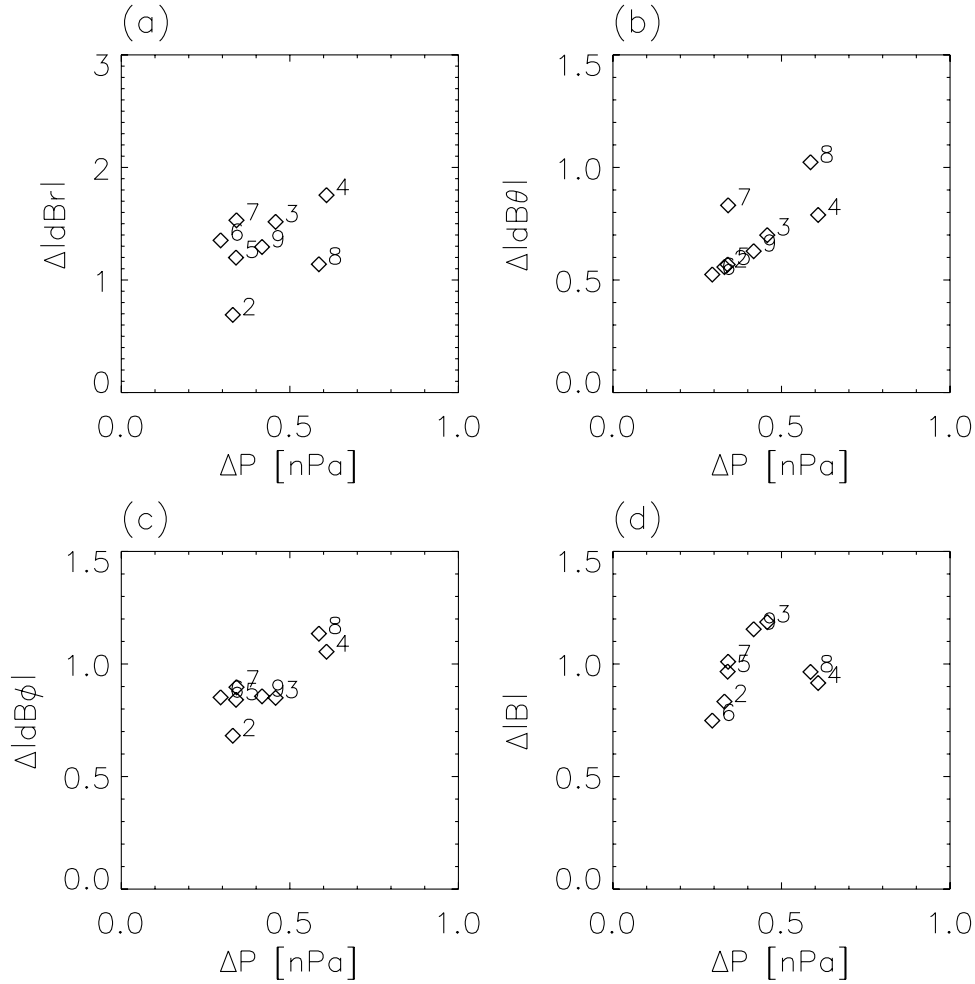

Figure 7. Scatter plots of maximum values of magnetic field disturbances in (a)B_r, (b)B_θ, (c)B_ϕ, and (d) |B| versus maximum values of solar wind dynamic pressure enhancements. The number attached to each diamond corresponds to the event number.

amplitudes of ULF disturbances in the B_r, B_θ, and B_ϕ components and |B| during 3 days before and after the arrival of the pressure enhancement. We choose the maximum values rather than the average values due to the fact that the averaged value is largely affected by the Galileo's location and chances for the current sheet crossing because observed disturbances in the current sheet are usually stronger than those in the lobe region. Positive correlation is clearly found in Figure 7 in all of the three components. Event 1 is omitted in Figure 7 because Galileo was located in the vicinity and sometimes outside the magnetopause at that time. The amplitudes of ULF disturbances of events 7 and 8 are relatively greater than those of other events as shown in Figure 7b, implying that there is a significant dawn-dusk asymmetry.

[22] Several spikes are observed in the magnetic field waveforms. For example, two spikes are seen on 21 October 1997 in Figure 6h, the first one with a polarity of $B_\theta < 0$ and the second one with a polarity of $B_\theta > 0$. A spike signature affects the enhancement in a vast range of the frequency space when the FFT is applied. In this study the FFT result contains these spikes' effects because a critical distinction between the spike and original ULF wave is unclear. This would cause the significant strengthening in events 7 and 8 as shown in Figure 7b.

[23] The spike signature is interpreted as the manifestation of reconnection [*Russell et al.*, 1998, 2000]. It is worthwhile to note that the tail reconnection and the following plasmoid eruption analogous to terrestrial substorm phenomena have been detected and investigated in the midnight to dawnside region of the Jovian magnetosphere by several researchers [*Russell et al.*, 1998, 2000; *Woch et al.*, 2002; *Cowley et al.*, 2003b].

[24] We propose that the magnetospheric compression causes the enhancement of the ULF disturbances through generating reconnection bursts. The reconnection rate should increase in the response to an arrival of pressure enhancement to release the enhanced potential energy in a compressed magnetosphere as reported by a simulation study [*Miyoshi and Kusano*, 2001]. This release of increased potential energy is associated with the increased current density expected to flow within the sheet during a compressed state as seen in simulation results by *Walker and Ogino* [2003]. The reconnection burst promotes the

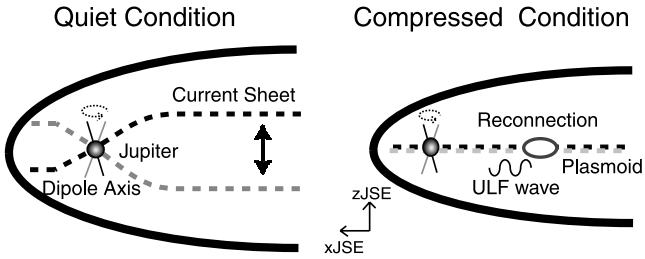

Figure 8. Schematic sketch for explaining the disappearance of magnetic field rectangular waveform during solar wind dynamic pressure enhancements (compressed condition). Bold black lines indicate the magnetopause on the JSE X-Z plane. Dashed lines represent the northernmost and southernmost locations of the current sheet. Generated plasmoid and ULF disturbances associated with reconnection are also shown.

intermittent plasmoid eruptions which are observed as spikes in the waveform [*Russell et al.*, 1998, 2000] and presumably enhances several kinds of ULF waves themselves via the plasma instabilities associated with the reconnection. This hypothesis is consistent with our results of a positive correlation between the maximum ULF power and the maximum pressure with a dawn-dusk asymmetry as shown in Figure 7b. The amplification in the B_r and |B| components as shown in Figures 6c, 6d, 6e, 6g, 6h, and 6i is also consistent with this hypothesis because such enhancement can be interpreted as the result of the sheet current enhancement.

[25] Disappearance of the rectangular waveform can be interpreted as a manifestation of the current sheet deformation. Assuming that the compressed magnetosphere becomes more dependent on the flow direction of the solar wind and that the current sheet approaches JSE $z = 0$ plane while solar wind dynamic pressure is extremely enhanced, Galileo will not experience the current sheet crossings, which causes the disappearance of the rectangular waveform, as schematically depicted in Figure 8. This hypothesis is consistent with the fact that when Galileo was located on the north (south) side of geographic equator, the magnetic field B_r component tended to be kept positive (negative). For example, judging from the z component of Galileo location in Table 1, Galileo was located on the north (south) side during events 6–9 (events 1–5). Except for event 5, our hypothesis is valid, i.e., B_r keeps its sign negative during events 1–4, while it keeps positive during events 7–9. Increasing of |B| in both lobe regions is confirmed for each event compared with the empirical model reported by *Kivelson and Khurana* [2002]. We suppose this variation is consistent with our suggestion because the increasing of lobe magnetic pressure could cause the deformation of the current sheet.

[26] *Khurana* [2001] suggested that the amplitude of the current sheet motion is estimated to reach several R_J in the north-south direction, while Galileo was located at JSE $z < 1$

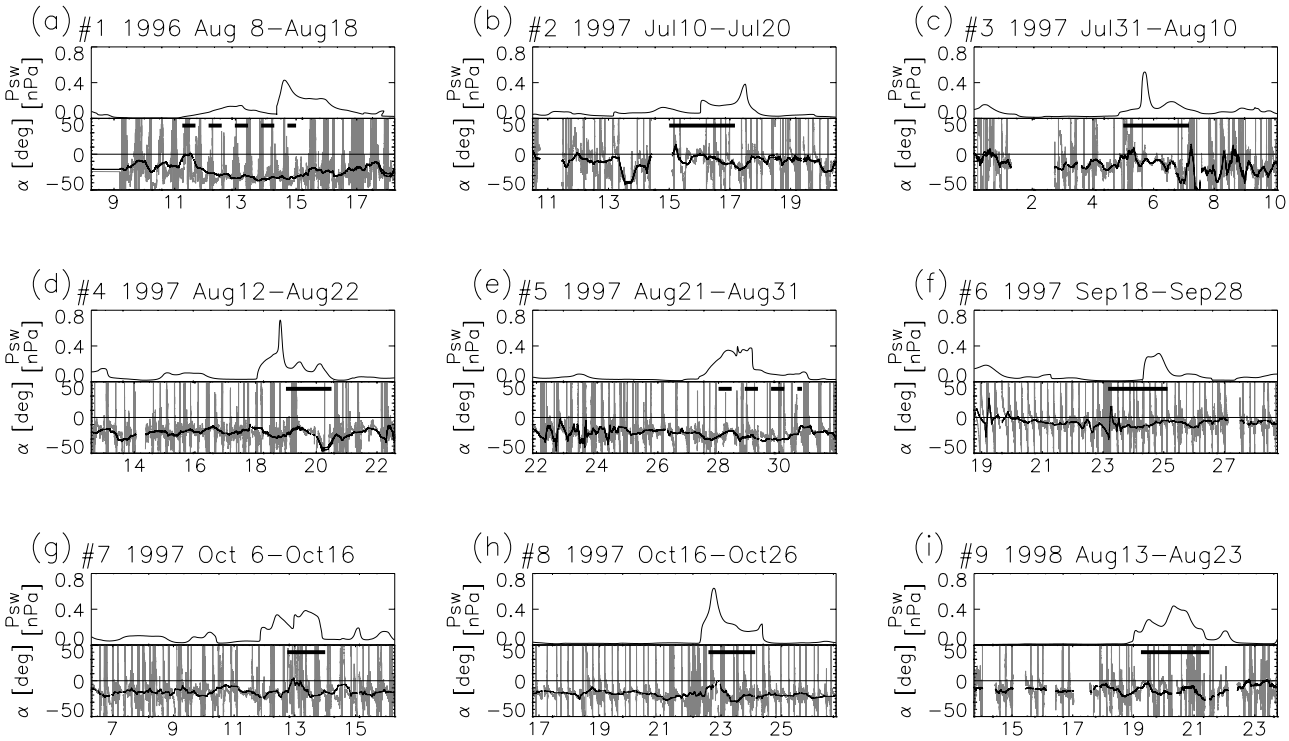

Figure 9. Time series plots of (top) the solar wind dynamic pressure obtained from the MHD simulation and (bottom) the α representing the "lead" (by $\alpha > 0$) or "lagging" (by $\alpha < 0$) of magnetic field. The lighter and darker traces are obtained from high-resolution (24 s) data and the boxcar averaged data for one planetary period, 10 hours, respectively. Black horizontal bars indicate the terms when the characteristic changes (described in the text) are observed. The dotted black bars indicate the unclear changes. (a), (b), . . ., (i) Corresponds to events 1, 2, . . ., 9, respectively, as in Figure 6.

R_J during events 2–9. Large decreasing in the amplitude of the current sheet motion is required for the absence of Galileo's current sheet crossing. Inconsistent changes are sometimes found; for example, in event 5, the current sheet moves southward while Galileo was located at JSE $z < 0$. The northward or southward displacement of an average location of the current sheet under the compressed condition is one of possible explanations for the disappearance of the rectangular waveform [*Russell*, 2001]. Further discussion for this problem will be reported in the future.

[27] In addition to the magnetic field variation in the north-south direction, we investigate changes in the corotational direction. It is important for considering the magnetosphere-ionosphere coupling to monitor the behavior of corotating plasma in the Jovian magnetosphere [*Hanlon et al.*, 2004]. Assuming that the magnetic field is "frozen in" to the magnetospheric plasma, "lag" or "lead" of plasma movement from the corotation can be judged from the angle $\alpha = \arctan(B_\phi/B_r)$. Figure 9 shows time series plots of α and predicted solar wind dynamic pressure. A positive (negative) increase in α represents an increase (decrease) in the angular velocity of the magnetic field and plasma. *Hanlon et al.* [2004] applied this analysis to the case study during the Cassini flyby as shown in their Figure 2g. They reported a positive increase in α for 1 Earth day followed by a negative increase corresponding to an arrival of a solar wind pressure pulse. Similar characteristic changes, positive and negative increases of α, are detected in almost all events as indicated by horizontal bars in Figure 9 and clearly at least for seven of the nine events (events 2–4 and 6–9).

[28] As discussed by *Hanlon et al.* [2004], these positive and negative increases in α would be interpreted as a clear manifestation of plasma's supercorotation and lagging caused by magnetospheric compression and expansion, respectively, which are consistent with the concept of conservation of angular momentum as suggested theoretically [*Southwood and Kivelson*, 2001; *Cowley et al.*, 2003a]. Although this theory was explained as the behavior of the plasma in the middle magnetosphere, this response is detected around 100 R_J where Galileo was located. For the events without clear signatures in α, Galileo was located dawnside at large distance from Jupiter (>115 R_J). In this dawnside region, plasma motion is normally far from corotation due to the effect of solar wind flow [*Khurana*, 2001].

6. Conclusions

[29] The response of the Jovian magnetosphere to solar wind dynamic pressure enhancements has been investigated using Galileo magnetometer data and solar wind parameters just upstream of Jupiter obtained from a solar wind MHD simulation. In response to the arrival of solar wind dynamic pressure enhancements, enhanced ULF disturbances and disappearance of usual magnetic field rectangular waveform are detected. We propose that a burst of magnetotail reconnection and a change in the position of the current sheet are plausible explanations for these two responses, respectively. A signature such as leadings of magnetic field angle followed by laggings, which is consistent with theoretical suggestions, is detected in almost all events but unclear for the events at >115 R_J in the dawn sector.

[30] **Acknowledgments.** We acknowledge all the working teams and PIs of IMP-8, WIND, ACE, Ulysses, and Galileo for the use of their precious data. We thank the excellent websites of OMNIWeb, COHOWeb, and PDS for helpfully supplying data from IMP-8; WIND; and ACE, Ulysses, and Galileo, respectively. CANS is supported by the Research and Development for Applying Advanced Computational Science and Technology (ACT-JST) program.

[31] Lou-Chuang Lee thanks Paul Hanlon and another reviewer for their assistance in evaluating this paper.

References

Cowley, S. W. H., E. J. Bunce, and J. D. Nichols (2003a), Origins of Jupiter's main oval auroral emissions, *J. Geophys. Res.*, *108*(A4), 8002, doi:10.1029/2002JA009329.

Cowley, S. W. H., E. J. Bunce, T. S. Stallard, and S. Miller (2003b), Jupiter's polar ionospheric flows: Theoretical interpretation, *Geophys. Res. Lett.*, *30*(5), 1220, doi:10.1029/2002GL016030.

Glassmeier, K.-H. (1995), Ultralow-frequency pulsations: Earth and Jupiter compared, *Adv. Space Res.*, *16*, 209–218.

Gurnett, D. A., et al. (2002), Control of Jupiter's radio emission and aurorae by the solar wind, *Nature*, *415*, 985–987.

Hanlon, P. G., M. K. Dougherty, N. Krupp, K. C. Hansen, F. J. Crary, D. T. Young, and G. Tóth (2004), Dual spacecraft observations of a compression event within the Jovian magnetosphere: Signatures of externally triggered supercorotation?, *J. Geophys. Res.*, *109*, A09S09, doi:10.1029/2003JA010116.

Joy, S. P., M. G. Kivelson, R. J. Walker, K. K. Khurana, C. T. Russell, and T. Ogino (2002), Probabilistic models of the Jovian magnetopause and bow shock locations, *J. Geophys. Res.*, *107*(A10), 1309, doi:10.1029/2001JA009146.

Khurana, K. K. (1992), A generalized hinged-magnetodisc model of Jupiter's nightside current sheet, *J. Geophys. Res.*, *97*(A5), 6269–6276.

Khurana, K. K. (2001), Influence of solar wind on Jupiter's magnetosphere deduced from currents in the equatorial plane, *J. Geophys. Res.*, *106*(A11), 25,999–26,016.

Kivelson, M. G., and K. K. Khurana (2002), Properties of the magnetic field in the Jovian magnetotail, *J. Geophys. Res.*, *107*(A8), 1196, doi:10.1029/2001JA000249.

Kivelson, M. G., K. K. Khurana, J. D. Means, C. T. Russell, and R. C. Snare (1992), The Galileo magnetic-field investigation, *Space Sci. Rev.*, *60*(1–4), 357–383.

Miyoshi, T., and K. Kusano (2001), A global MHD simulation of the Jovian magnetosphere interacting with/without the interplanetary magnetic field, *J. Geophys. Res.*, *106*(A6), 10,723–10,742.

Russell, C. T. (2001), The dynamics of planetary magnetosphere, *Planet. Space Sci.*, *49*, 1005–1030.

Russell, C. T., K. K. Khurana, D. E. Huddleston, and M. G. Kivelson (1998), Localized reconnection in the near Jovian magnetotail, *Science*, *280*, 1061–1064.

Russell, C. T., K. K. Khurana, M. G. Kivelson, and D. E. Huddleston (2000), Substorms at Jupiter: Galileo observations of transient reconnection in the near tail, *Adv. Space Res.*, *26*, 1499–1504.

Smith, E. J., R. W. Fillius, and J. H. Wolfe (1978), Compression of Jupiter's magnetosphere by the solar wind, *J. Geophys. Res.*, *83*, 4733–4742.

Southwood, D. J., and M. G. Kivelson (2001), A new perspective concerning the influence of the solar wind on the Jovian magnetosphere, *J. Geophys. Res.*, *106*(A4), 6123–6130.

Vennerstrom, S., N. Olsen, M. Purucker, M. H. Acuña, and J. C. Cain (2003), The magnetic field in the pile-up region at Mars, and its variation with the solar wind, *Geophys. Res. Lett.*, *30*(7), 1369, doi:10.1029/2003GL016883.

Walker, R. J., and T. Ogino (2003), A simulation study of currents in the Jovian magnetosphere, *Planet. Space Sci.*, *51*, 295–307.

Woch, J., N. Krupp, and A. Lagg (2002), Particle bursts in the Jovian magnetosphere: Evidence for a near-Jupiter neutral line, *Geophys. Res. Lett.*, *29*(7), 1138, doi:10.1029/2001GL014080.

H. Fukunishi, Y. Takahashi, and C. Tao, Department of Geophysics, Tohoku University, Sendai, Miyagi, 980-8578, Japan. (tao@pat.geophys.tohoku.ac.jp)

R. Kataoka, National Institute of Information and Communications Technology, Koganei, Tokyo, 184-8795, Japan.

T. Yokoyama, Department of Earth and Planetary Science, University of Tokyo, Bunkyo-ku, Tokyo, 113-0033, Japan.